Soft Matter

ARTICLE TYPE

Cite this: DOI: 00.0000/xxxxxxxxxx

pH response of sequence-controlled polyampholyte brushes †

Xin Yuan, Harold W. Hatch, *b Jacinta C. Conrad, Amanda B. Marciel, and Jeremy C. Palmer, *a

Received Date Accepted Date

DOI: 00.0000/xxxxxxxxxx

We use molecular simulation to investigate the pH response of sequence-controlled polyampholyte brushes (PABs) with polymer chains consisting of alternating blocks of weakly acidic and basic monomers. Changes in the ionization state, height, lateral structure, and chain conformations of PABs with pH are found to differ qualitatively from those observed for polyelectrolyte brushes. Grafting density has a relatively modest effect on PAB properties. By contrast, monomer sequence strongly affects the pH response, with the extent of the response increasing with the block size. This trend is attributed to strong electrostatic attractions between oppositely charged blocks, which lead to an increase in chain backfolding as block size increases. This behavior is consistent with that observed for polyampholytes with similar monomer sequences in solution in previous studies. Our study shows that monomer sequence can be used to tune the pH response of weak PABs to generate stimuli-responsive surfaces.

1 Introduction

Polymers may be anchored to spherical and planar surfaces forming brush architectures to tune complex materials properties including mechanical strength, wetting, adhesion, lubrication, compatibilization, anti-coagulation, and anti-fouling for applications in separations, energy storage/conversion, and biotechnology. 1-5 The properties manifested at the interface are dependent on polymer brush conformation, which is influenced by chain length, grafting density, and monomer chemistry, as well as the ion and proton concentration present in the brush. Polyelectrolyte brushes (PEBs), in particular, exhibit unique behavior compared to systems with neutral polymers. The competition between repulsive (electrostatic and excluded volume) monomer interactions and elastic forces that oppose chain stretching leads to transitions between collapsed and extended brush conformations as solution conditions (e.g., salt concentration and pH) are varied, resulting in surfaces that are responsive to external stimuli.

Additional surface functionality may gained by using polymers that contain both positive and negative charges called polyamPABs and zwitterionic systems have largely been investigated for their anti-fouling behavior. 9–12 Solid-phase synthesis strategies have enabled precise control over molecular weight and the sequence of charged monomers along the chain in PABs consisting of polypeptides or polypeptoids. These studies found that anti-fouling behavior is dependent on a combination of charge sequence, ionic concentration, and grafting density, where sequences with alternating charge groups generally exhibited enhanced anti-fouling properties. 13–20 It is posited that the physicochemical properties of PABs will be strongly dependent on charge monomer sequence, similar to polyampholyte solution behavior. 21

Various computational and theoretical approaches have been applied to investigate the influence of monomer sequence and other variables on the properties of PABs. ^{22–26} However, these studies have focused on sequence-controlled PABs with strong acid and base chemistries in which the monomers remain fully ionized under typical solution conditions or employed methods

pholytes or polyzwitterions. Due to the presence of attractive and repulsive electrostatic intra-chain interactions, charge-neutral polyampholyte brushes (PABs) and zwitterionic systems exhibit more complex conformational behavior compared to PEBs. For example, PABs show swelling behavior in ionic solutions making them applicable in ion-rich environment and biological systems as viscosity modifiers, drag reducers, and adsorption materials. ^{6,7} This "antipolyelectrolyte" effect was recently observed for a zwitterionic brush containing amino acid moieties in the presence of monovalent ions. ⁸

 $[^]a$ Department of Chemical and Biomolecular Engineering, University of Houston, Houston. TX 77204

^b Chemical Sciences Division, National Institute of Standards and Technology, Gaithersburg, Maryland 20899-8320

 $^{^{}c}$ Department of Chemical and Biomolecular Engineering, Rice University, Houston, Texas 77005

 $^{^{*}}$ E-mails: harold.hatch@nist.gov, jcconrad@uh.edu, am152@rice.edu, jc-palmer@uh.edu

[†] Electronic Supplementary Information (ESI) available: See DOI: 10.1039/cXsm00000x/

that assume fixed monomer charge states. By contrast, PABs with weakly acidic and basic monomers exhibit changes in their charge state due to variations in pH and salt concentration and hence enhanced brush responses that can be harnessed to design smart surfaces. For example, a recent study using a mean-field molecular theory found that variations in pH, salt concentration, and solvent quality can induce complex nonomonomic changes in brush height and lateral microphase separation in weak PABs with diblock sequences. ²⁷ Nonetheless, the properties of weak PABs have not been extensively studied and thus fundamental understanding of the effects of monomer sequence and other key physical variables on their behavior remains incomplete.

Here, we use molecular simulation to study the pH response of coarse-grained models of sequence-controlled PABs with different grafting densities, focusing on polymer chains with alternating blocks of weakly acidic and basic monomers. Charge regulation in the brushes is modeled using the recently developed grand reaction method (GRM) for simulating acid-base equilibrium, which rigorously accounts for the effects of solution conditions and local environment on monomer ionization. The PABs are characterized by analyzing their ionization state, height, lateral structure, and chain conformations. These metrics reveal that the pH response of PABs is qualitatively different from brushes consisting of weak poly-acid or -base homopolymers. Moreover, whereas grafting density has a modest effect on the properties of PABs, their behavior is found to depend sensitively on monomer sequence, with systems with larger block sizes exhibiting more pronounced response to changes in pH. These results indicate that monomer sequence can be tuned to control behavior of weak PABs, enabling the design of smart, stimuli-responsive surfaces.

2 Methods

2.1 Brush and solution models

Simulations were performed using ESPResSo 4.1.4²⁸ to study the effects of monomer sequence and grafting density on the response of planar weak PABs to changes in pH. We adopted a coarsegrained model similar to those that have been used to successfully describe the phase behavior, structure, and long-time equilibrium (Rouse) dynamics of charged polymers, vielding predictions in good qualitative (and often semi-quantitative) agreement with experiment. 29-34 As described below, the coarse-grained polymers were modeled as linear bead-spring chains. Each monomer is represented as a single bead and assigned an identity of glutamic acid (E) or lysine (K). The E and K monomers are ionizable acidic (A) and basic (B) species, respectively. Acid and base reactions involving the monomers (HA \rightleftharpoons A⁻ + H⁺ and $B \rightleftharpoons HB^+ + OH^-$, respectively) were simulated explicitly using the grand-reaction method. 35-37 Thus, the monomer beads can be neutral or carry a charge at any given instant in the simulation, depending on their identity, the solution conditions, and the local environment. Free solution ions, including Na⁺ and Cl⁻, as well as the H⁺ and OH⁻ species involved in the acid/base reactions, were modeled as single charged beads, whereas the background solvent (water) is treated as a dielectric continuum. For convenience, the model parameters and physical quantities from the simulations are reported using fundamental units of σ , m, and $k_{\rm B}T$ for length, mass, and energy, respectively, where $k_{\rm B}$ is the Boltzmann constant and T is temperature.

The model PABs consist of M identical linear chains, each with $N_{\rm m}=48$ monomers and the same K-E monomer sequence. Following recent studies of sequence-controlled polyampholytes in solution, ^{38–40} we considered polymer chains with different K and E block sizes ranging from K₂₄E₂₄ (diblock) to (KE)₂₄ (alternating) (Table 1). For comparison, we also examined the behavior of PEBs consisting of homopolymers with sequences K₄₈ and E₄₈ (Table 1). The chains were end-grafted onto an uncharged surface in the x-y plane by fixing the positions of one of their terminal beads (the terminal E for the polyampholytes) at $z = 1\sigma$ on a square lattice with areal density ρ and spacing $d = \rho^{-1/2}$ (Fig. 1). The brushes were embedded in a simulation cell with an infinite, two-dimensional slab geometry and $x \times y \times z$ dimensions of $L_x \times L_y \times L_z$, where $L_x = L_y = L = (M/\rho)^{1/2}$ and $L_z = 2N_{\rm m}\sigma$. The slab geometry was created by imposing periodic boundary conditions along the x and y directions and placing bounding lower and upper walls at z = 0 and $z = L_z$, respectively. For each polymer sequence, we simulated brushes with three different grafting densities $\{0.01, 0.04, 0.09\}$ σ^{-2} . These values span the range encountered in typical syntheses 41-43 and the physical regime where adjacent chains in the model brush systems transition from weakly to strongly interacting, as determined by analyzing lateral fluctuations parallel to the grafting surface via the in-plane radius of gyration $\langle R_{g,xy}^2 \rangle^{1/2}$. We used $M = \{64, 81, 144\}$ polymer chains for the three grafting densities, respectively, to ensure that the xand y-dimensions of the simulation cells were sufficiently large $(L \gtrsim 35\sigma \gg \langle R_{\rm g,xy}^2 \rangle^{1/2})$ to minimize spurious finite size effects.

Excluded volume interactions between all particles (polymer monomers and free solution ions) were modeled using the Weeks-Chandler-Andersen (WCA) potential, 44

$$U_{\text{WCA}}(r_{ij}) = \begin{cases} 4\varepsilon \left\{ \left(\frac{\sigma_{ij}}{r_{ij}}\right)^{12} - \left(\frac{\sigma_{ij}}{r_{ij}}\right)^{6} + \frac{1}{4} \right\}, & \text{if } r_{ij} < 2^{\frac{1}{6}}\sigma_{ij} \\ 0, & \text{if } r_{ij} \ge 2^{\frac{1}{6}}\sigma_{ij} \end{cases}$$

$$(1)$$

where r_{ij} is the scalar distance between particles i and j, and parameters $\varepsilon = k_B T$ and $\sigma_{ij} = \sigma$ set the interaction strength and length scale, respectively. Thus, all particles have the same effective size, and excluded volume interactions between all species types are identical. Bonded interactions between neighboring monomers along each chain were described by the finite extensible nonlinear elastic (FENE) potential, 45,46

$$U_{\text{FENE}}(r) = \begin{cases} -\frac{1}{2}k_{\text{bond}}\Delta r_{\text{max}}^2 \ln\left(1 - \left(\frac{r}{\Delta r_{\text{max}}}\right)^2\right), & \text{if } r < \Delta r_{\text{max}} \\ \infty, & \text{if } r \ge \Delta r_{\text{max}} \end{cases}$$

where $k_{\rm bond}=30k_{\rm B}T/\sigma^2$ is the bond stiffness and $\Delta r_{\rm max}=1.5\sigma$ is the maximum bond length.

Electrostatic interactions between charged particles were modeled via the Coulomb potential,

$$U_{\rm C}(r_{ij}) = \lambda_{\rm B} k_{\rm B} T \frac{z_i z_j}{r_{ij}} \tag{3}$$

Abbreviation	Sequence
K ₄₈	K-K-K-K-K-K-K-K-K-K-K-K-K-K-K-K-K-K-K-
E_{48}	E-E-E-E-E-E-E-E-E-E-E-E-E-E-E-E-E-E-E-
$K_{24}E_{24}$	K-K-K-K-K-K-K-K-K-K-K-K-K-K-K-K-K-K-K-
$(K_{12}E_{12})_2$	K-K-K-K-K-K-K-K-K-K-K-E-E-E-E-E-E-E-E-E
$(K_6E_6)_4$	K-K-K-K-K-E-E-E-E-E-E-K-K-K-K-K-K-E-E-E-E-E-E-E-K-K-K-K-K-E-E-E-E-E-E-K-K-K-K-K-E
$(K_4E_4)_6$	K-K-K-E-E-E-E-K-K-K-E-E-E-E-K-K-K-K-E-E-E-E-K-K-K-K-E-E-E-E-K-K-K-K-E-E-E-E-K-K-K-K-E
$(K_3E_3)_{12}$	K-K-K-E-E-E-K-K-K-E-E-E-K-K-K-E-E-E-K-K-K-E-E-E-K-K-K-E-E-E-K-K-K-E-E-E-K-K-K-E-E-E-K-K-K-E-E-E-E-K-K-K-E-E-E-E
$(K_2E_2)_{24}$	K-K-E-E-K-K-E-E-K-K-E-E-K-K-E-E-K-K-E-E-K-K-E-E-K-K-E-E-K-K-E-E-K-K-E-E-K-K-E-E-K-K-E-E-K-K-E-E-K-K-E-E-K-K-E-E
$(KE)_{24}$	K-E-K-E-K-E-K-E-K-E-K-E-K-E-K-E-K-E-K-E

Table 1 Sequences of glutamic acid (E) and lysine (K) monomers examined in this study.

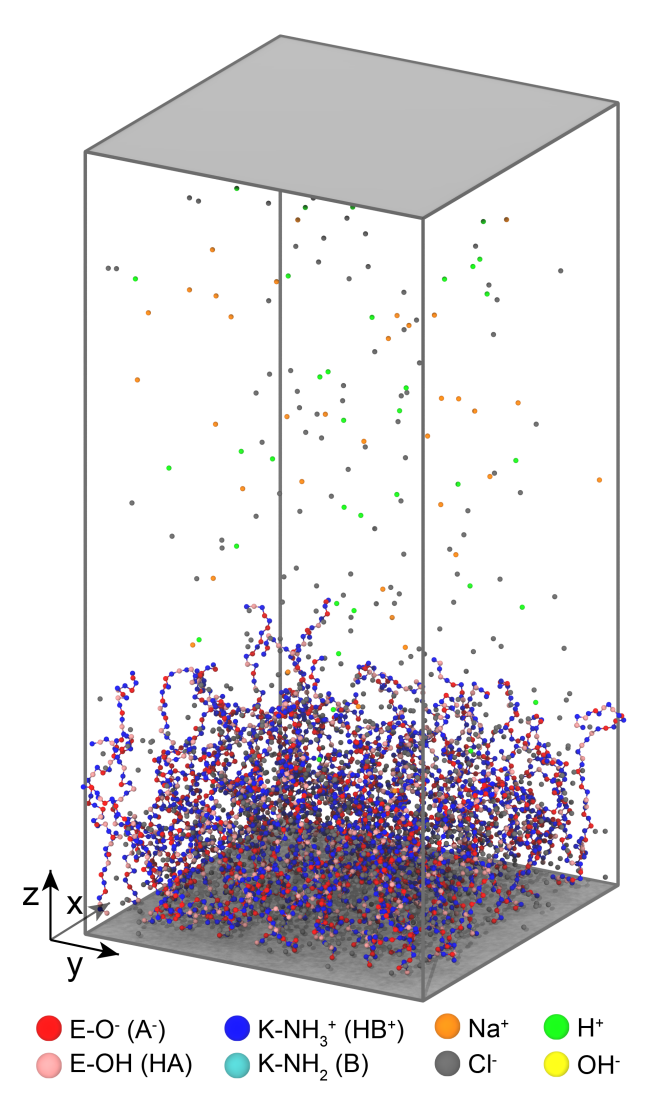


Fig. 1 Model PAB with monomer sequence $(KE)_{24}$ and grafting density $\rho=0.04\sigma^{-2}$. The dimensions of the system are $L_x=L_y=45\sigma$ and $L_z=96\sigma$. Grey surfaces are the lower and upper walls at z=0 and $z=L_z$, respectively. The brush is in equilibrium with a bulk reservoir with pHres = 2 and salt concentration $c_{\rm salt}^{\rm res}=0.01$ M. The paucity of $K-{\rm NH}_2$ (B) and OH $^-$ species is due to the acidic conditions of the system.

where z_i and z_j are the charge numbers of particles i and j, and $\lambda_{\rm B}=2\sigma$ is the Bjerrum length. For water at room temperature, $\lambda_B \approx 0.71$ nm, which implies that $\sigma \approx 0.355$ nm, establishing a connection between the physical length scales in simulation and experiment. Long-range contributions to the electrostatic interactions were treated using a three dimensional particle-particleparticle-mesh (P3M) solver in conjunction with the electrostatic layer correction (ELC). 47-49 The ELC accounts for the aperiodicity of the two-dimensional slab geometry of the simulation cell by adding a vacuum gap in the z-dimension and applying a correction to the standard P3M method to cancel interactions between neighboring images along this direction. The simulations were preformed using a standard gap size of $L_{\rm ELC} = 0.2L_z$, and other parameters, including the cutoff for the Coulomb potential, were chosen to ensure a relative error of 10^{-5} in the computed electrostatic forces. 47-49

2.2 Acid-base equilibrium

Acid-base equilibrium in the brush systems was modeled using the grand-reaction method. ^{35–37} This approach combines reaction ensemble ^{50,51} and grand canonical ^{52,53} Monte Carlo moves to model acid-base equilibrium in a system coupled to an external reservoir with a specified pH and salt concentration, rigorously accounting for the Donnan partitioning of free solution ions between the two phases. Additionally, the GRM's reformulation of the standard ionization reactions to explicitly incorporate other solution species facilitates simulation across a broader range of pH and salt concentrations than alternative approaches such as standard reaction ensemble Monte Carlo ^{35,51} or the constant-pH method. ⁵⁴ We note these advantages of the GRM are also realized in the recently proposed charge regulation Monte Carlo method. ⁵⁵ Detailed descriptions of the GRM and these alternative approaches are given in Refs. 35 and 56.

Briefly, consider a system containing weakly acidic (A) and basic (B) species with intrinsic disassociation constants pK_A^{acid} and pK_A^{base} , respectively, in equilibrium with an aqueous reservoir with free solution ion concentrations c_i^{res} for species $i \in \{\text{Na}^+, \text{Cl}^-, \text{H}^+, \text{OH}^-\}$. The acidic species are involved in the fol-

lowing reactions:

$$\mathrm{HA} \rightleftharpoons \mathrm{A}^- + \mathrm{H}^+ \qquad \qquad K_{\mathrm{A}} = 10^{-pK_{\mathrm{A}}^{\mathrm{acid}}} \qquad \qquad \text{(4)}$$

$$\mathrm{HA} + \mathrm{OH}^- \rightleftharpoons \mathrm{A}^- \qquad \qquad K_A' = \frac{K_\mathrm{A}}{K_\mathrm{CU}}$$
 (5)

$$HA \rightleftharpoons A^- + Na^+$$
 $K''_A = K_A \frac{c^{\text{res}}_{Na^+}}{c^{\text{res}}_{H^+}}$ (6)

$$HA + Cl^{-} \rightleftharpoons A^{-} \qquad K_{A}^{"'} = \frac{K_{A}c_{OH^{-}}^{res}}{K_{W}c_{Cl^{-}}^{res}}, \qquad (7)$$

where the various K denote solution-phase reaction equilibrium constants and $K_{\rm w}=10^{-{\rm p}K_{\rm w}}$ is the ion product for water. The reactions for the base are:

$$B \rightleftharpoons HB^+ + OH^- \qquad K_B = 10^{-(pK_w - pK_A^{base})}$$
 (8)

$$B + H^{+} \rightleftharpoons HB^{+}$$
 $K_{B}^{'} = \frac{K_{B}}{K_{W}}$ (9)

$$B \rightleftharpoons HB^{+} + Cl^{-}$$
 $K_{B}^{"} = K_{B} \frac{c_{Cl^{-}}^{res}}{c_{OH^{-}}^{res}}$ (10)

$$B + Na^+ \rightleftharpoons HB^+$$
 $K_B^{""} = \frac{K_B c_{H^+}^{res}}{K_W c_{Na^+}^{res}}.$ (11)

The reactions in Eqs. 4-7 are not independent but a reformulation of the typical form for acids (Eq. 4) using other solution species. Similarly, Eqs. 8-11 are a reformulation of the standard form (Eq. 8) for bases. Additionally, we note that the equations for the equilibrium constants in Eqs. 6, 7, 10, and 11 are final, simplified expressions derived by imposing electroneutrality of the reservoir. ³⁵

Lastly, equilibrium with the reservoir is maintained through the following auxiliary reactions:

$$H^+ \rightleftharpoons Na^+ \qquad K_{Na-H} = \frac{c_{Na^+}^{res}}{c_{H^+}^{res}}$$
 (12)

$$OH^{-} \rightleftharpoons CI^{-} K_{Cl-OH} = \frac{c_{Cl^{-}}^{res}}{c_{OH^{-}}^{res}} (13)$$

$$\emptyset \rightleftharpoons \mathrm{Na^+} + \mathrm{Cl^-} \qquad K_{\mathrm{Na+Cl}} = c_{\mathrm{Na}^+}^{\mathrm{res}} c_{\mathrm{Cl}^-}^{\mathrm{res}} \exp \left[\frac{\mu_{\mathrm{ex}}(I^{\mathrm{res}})}{kT} \right]$$
 (14)

where $\mu_{\rm ex}(I^{\rm res})$ is the excess chemical potential for a neutral ion pair in the reservoir and $I^{\rm res}=\frac{1}{2}\sum_i z_i^2 c_i^{\rm res}$ is the ionic strength.

The reaction network involves acid-base reactions (Eqs. 4-7 and 8-11) as well as auxiliary identity change (Eqs. 12 and 13) and ion pair insertion/deletion (Eq. 14) "reactions" that impose equilibrium with the reservoir. The network is fully determined by specifying remaining model parameters $pK_A^{\rm acid}$ and $pK_A^{\rm base}$ and physical parameters pK_W , T, $pH^{\rm res}$ ($c_{H^+}^{\rm res}$ or $c_{OH^-}^{\rm res}$), and $c_{\rm salt}^{\rm res}$. All simulations reported in this study were performed using $pK_A^{\rm acid} = 4.4$ and $pK_A^{\rm base} = 10.4$ for glutamic acid (E) and lysine (K) monomer beads, 57,58 respectively, $pK_W = 14$, $T = 1/k_B$, and $c_{\rm salt}^{\rm res} = 0.01$ M; the pH was varied across different simulations as an independent parameter. This low salt concentration is insufficient to fully screen electrostatic interactions within the brushes and was cho-

sen to compare with the "osmotic" regime, where the brush height of weak PEBs is predicted to increase with increasing salt concentration. 27

The excess chemical potential $\mu_{\rm ex}(I^{\rm res})$ in Eq. 14 was calculated from molecular dynamics (MD) simulations of the bulk reservoir using the Widom test particle method 59,60 and numerical procedures identical to those reported in Ref. 35. The reservoir contained 400 NaCl ion pairs, and its size was varied between simulations to achieve different values of I^{res} . The function $\mu_{\text{ex}}(I^{\text{res}})$ obtained via interpolation of the data from the reservior simulations was then used to find the chemical potential and species concentrations c_i^{res} consistent with the specified pH and salt concentration $c_{\mathrm{salt}}^{\mathrm{res}}$. This procedure involved iteratively adjusting species concentrations, in a manner equivalent to adding NaOH or HCl to the reservoir, to find values of c_i^{res} and μ_{ex} that yielded the target pH and satisfied the constraints $K_{\rm W} = c_{\rm H^+}^{\rm res} c_{\rm OH^-}^{\rm res} \exp\left[\frac{\mu_{\rm ex}}{k_{\rm B}T}\right] = 10^{-14}$ and $\min(c_{\mathrm{Na^+}}^{\mathrm{res}}, c_{\mathrm{Cl^+}}^{\mathrm{res}}) = c_{\mathrm{salt}}^{\mathrm{res}}$. Finally, the resulting values of μ_{ex} and c_i^{res} were used to specify the reaction network (Eqs. 4-14) in the brush simulations and thus connect the systems to a reservoir with the desired pH and $c_{\text{salt}}^{\text{res}}$.

2.3 Sampling protocol

Following Ref. 35, properties of the model were sampled using a combination of MC and MD. Two types of MC moves were employed in this study. For each move type, the attempted transition between the old state (o) and new state (n) is accepted via the Metropolis-Hastings criterion: ⁶¹

$$P_{\text{o}\to\text{n}}^{\text{acc}} = \min\left\{1, \mathcal{C}\exp\left(-\beta\Delta U_{\text{on}}\right)\right\},\tag{15}$$

where $\Delta U_{\rm on} = U_{\rm n} - U_{\rm o}$ is the change in potential energy and $\mathscr C$ is a prefactor that depends on the type of move.

In a reaction MC move, ^{35,50,51} one of the forward or reverse reactions in Eqs. 4-14 is selected at random. The reaction is then attempted by replacing randomly selected reactant particles with the corresponding products. In this case,

$$\mathscr{C} = (K(c^{\ominus}VN_{\mathcal{A}})^{\bar{V}})^{\zeta} \prod_{i} \left[\frac{(N_{i}^{0})!}{(N_{i}^{0} + v_{i}\zeta)!} \right], \tag{16}$$

where *K* is the reaction equilibrium constant, c^{\ominus} is the standard reference concentration (1M), $V = L_x \times L_y \times L_z$ is the volume of the simulation cell, N_A is Avogadro's constant, ζ is the extent of reaction (+1 and -1 for forward and reverse reactions, respectively), N_i^0 is the particle number of species i before the proposed reaction, v_i is the stoichiometric coefficient of species i, $\bar{v} = \Sigma_i v_i$, and $\beta = 1/k_BT$. We note that the reaction MC moves for the auxiliary reactions in Eqs. 12-13 and Eq. 14 are formally equivalent to the identity exchange and ion pair insertion/deletion moves, respectively, that are commonly used in GCMC simulations. 53,62 Charge exchange MC moves were also performed between randomly selected monomers of the same E or K type. 63-65 These moves essentially swap the identity of $\{HA,A^-\}$ and $\{B,HB^+\}$ monomer pairs while keeping the number of each type of species and total charge constant. The exchanges expedite equilibration of the polymer charge distribution and are accepted using the criterion in Eq. 15 with $\mathcal{C} = 1$.

Sampling was performed by alternating MC and MD steps. The MC steps consisted of $2N_{\rm m}$ and $N_{\rm m}/10$ attempted reaction and charge exchange moves, respectively. The MD steps involved propagating a 1000 time steps trajectory in the canonical ensemble using the velocity Verlet algorithm with a $\delta t = 0.01\tau$ time step and a Langevin thermostat with friction coefficient $\gamma = \tau^{-1}$, where $\tau = \sigma(m/k_BT)^{1/2}$. The brush systems were equilibrated for 10⁴ MC-MD cycles, with each cycle consisting of one MC and one MD step. Equilibration was followed by a production period of 10⁴ MC-MD cycles, during which statistics were collected for subsequent analysis. Statistical uncertainties in each observable \mathscr{A} were estimated as $\langle \mathscr{A} \rangle \pm 2\sqrt{\operatorname{var}(\mathscr{A})/\tilde{n}_{\mathscr{A}}}$, where $\operatorname{var}(\mathscr{A}) = \langle \mathscr{A}^2 \rangle - \langle \mathscr{A} \rangle^2$ is the variance, $\tilde{n}_{\mathscr{A}} \approx n_{\mathscr{A}}/(2\tau_{\mathscr{A}})$ is the effective number of statistically independent samples, $n_{\mathcal{A}}$ is the total number of observations, and $\tau_{\mathscr{A}} \equiv \int_0^\infty C_{\mathscr{A}}(t) dt$ is the mean correlation time computed from the normalized auto-correlation function $C_{\mathscr{A}}(t) = (\langle \mathscr{A}(t)\mathscr{A}(0)\rangle - \langle \mathscr{A}^2\rangle) / \text{var}(\mathscr{A})$. The production phases of the simulation were sufficient in duration to yield $\tilde{n}_{\mathscr{A}} \gtrsim 50$ independent samples for each observable.

3 Results and Discussion

We first examine the titration curves for the brushes. The degree of ionization is defined as the fraction of acidic and basic species that are ionized:

$$\langle \alpha \rangle = \frac{c_{A^-} + c_{HB^+}}{c_{A^-} + c_{HA} + c_{HB^+} + c_B}.$$
 (17)

For a system of ideal (noninteracting) acidic and basic species, the degree of ionization is given by the Henderson-Hasselbalch (HH) equation:

$$\alpha_{\text{ideal}} = f_{\text{acid}} \alpha_{\text{ideal}}^{\text{acid}} + f_{\text{base}} \alpha_{\text{ideal}}^{\text{base}},$$
 (18)

where

$$\alpha_{\text{ideal}}^{\text{acid}} = \frac{10^{(\text{pH} - pK_A^{\text{acid}})}}{1 + 10^{(\text{pH} - pK_A^{\text{acid}})}},$$
(19)

$$\alpha_{\text{ideal}}^{\text{base}} = \frac{10^{(\text{pOH} - pK_B)}}{1 + 10^{(\text{pOH} - pK_B)}},$$
(20)

 f_{acid} and $f_{\text{base}} = 1 - f_{\text{acid}}$ are the fractions of acid and base species, $pOH = pK_W - pH$, and $pK_B = pK_W - pK_A^{\text{base}}$.

The titration curves, $\langle \alpha \rangle$, for the PEBs E₄₈ ($f_{\rm acid}=1$) and K₄₈ ($f_{\rm base}=1$) monotonically increase and decrease with pH^{res}, respectively (Fig. 2). Although these behaviors are qualitatively consistent with those predicted by the HH equation, significant quantitative deviations are observed. Similar deviations have been reported in a previous computational study of titration behavior of weak polyacids in solution using the GRM, where they were shown to primarily arise from two factors. ³⁵ First, the presence of ionizable polymers in the brush phase that cannot be exchanged with the reservoir results in Donnan partitioning of free solution ions and deviations between the effective pHs of the two phases (i.e., $c_i^{\rm res} \neq c_i^{\rm brush}$ and pH^{res} \neq pH^{brush} in general). ³⁵ Second, the ideality assumption used to derive the HH expressions is violated by the strong electrostatic interactions between charged species.

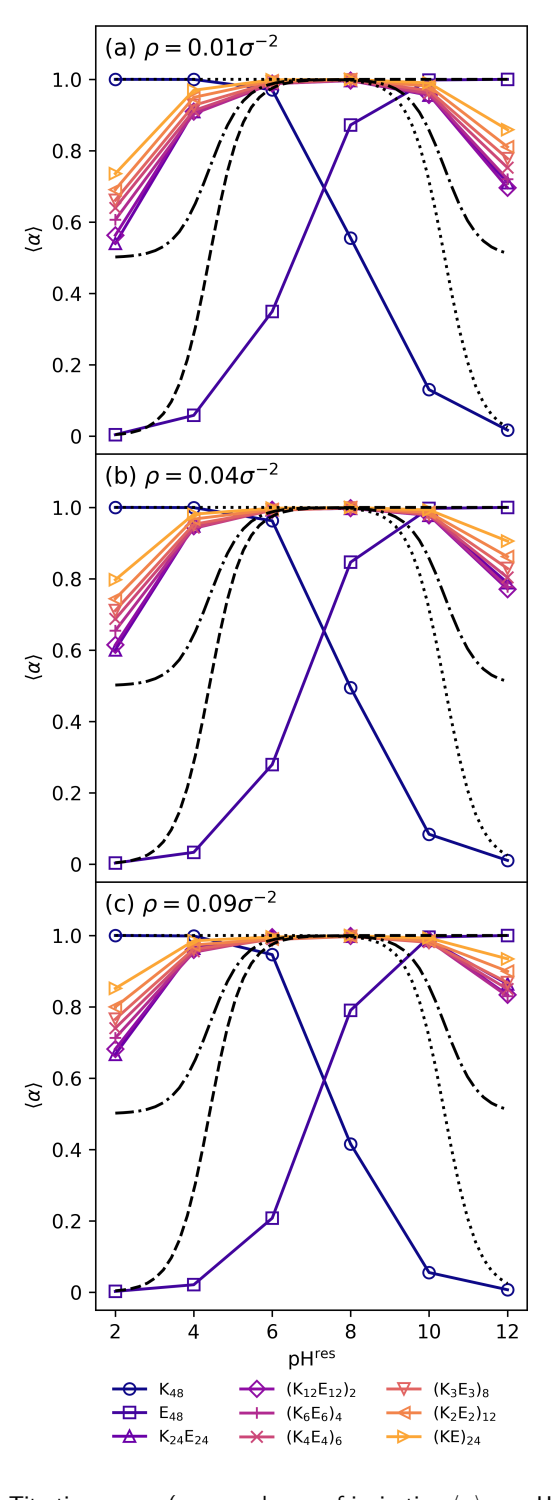


Fig. 2 Titration curves (average degree of ionization $\langle \alpha \rangle$ vs. pH^{res}) for brushes with different monomer sequences and grafting densities of $\rho=$ (a) 0.01, (b) 0.04, and (c) 0.09 σ^{-2} . Ideal Henderson-Hasselbalch titration curves (Eq. 18) are shown for $f_{acid}=1$ (dashed line), $f_{base}=1$ (dotted line), and $f_{acid}=f_{base}=0.5$ (dash-dotted line). Uncertainties are smaller than symbol size.

By contrast, the titration curves for the PABs ($f_{acid} = f_{base} = 0.5$) vary non-monotonically with pH^{res}. For pH^{res} $\approx 4-10$, $\langle \alpha \rangle \approx 1$, but it decreases sharply as pH^{res} moves outside this range. This behavior is qualitatively consistent with the HH prediction, though quantitative discrepancies are observed due to Donnan partitioning and the non-ideality of the systems. The non-monotonic trend arises because the PABs contain both weakly acidic and basic monomers (E and K, respectively) with comparable acid/base strength and in equal fractions. Thus, the majority of monomers are ionized near neutral pH^{res}, resulting in $\langle \alpha \rangle \approx 1$. As pH^{res} approaches either extreme, however, $\langle \alpha \rangle \to 0.5$ because half of the monomers will ionize and the other half will become neutral.

Monomer sequence also affects the titration behavior of the PABs. For pH^{res} $\approx 4 - 10$, $\langle \alpha \rangle$ is nearly independent of monomer sequence. Conversely, at both lower and higher values of pHres, $\langle \alpha \rangle$ increases as the block size is decreased from 24 to 1 (i.e., K₂₄E₂₄ to (KE)₂₄). Polyampholyte chains with smaller block sizes contain a greater number of charge-pattern interfaces where the sequence switches between K and E, 38 which are oppositely charged in their ionized states (i.e., A⁻ and HB⁺, respectively). Favorable electrostatic interactions arising from local charge pairing enhance the ionizability of monomers at the interfaces (Figs. S1 and S2 in ESI). The local electroneutrality also reduces free ion condensation near the charge interfaces (Fig. S3 in ESI). Thus, sequences with more charge-pattern interfaces exhibit a higher degree of ionization over a broader range of pH^{res} and lower overall coordination with free ions. These observations are consistent with those predicted by mean-field theories for PABs and polyampholytes in solution. 27,38

For the PEBs, increasing the grafting density ρ results in a slight decrease in $\langle \alpha \rangle$ over the range pH^{res} $\approx 4-10$. All of the monomers in the PEBs carry the same positive or negative charge in their ionized states, resulting in repulsive electrostatic interactions between monomers that must be screened by free counterions in solution (Fig. S3 and S4 in ESI). Increasing ρ enhances these repulsive interactions, making ionization less favorable at a given pH^{res}. ^{66,67} This decrease in $\langle \alpha \rangle$ with increasing grafting density is consistent with the behavior reported in simulations of weak polyacid chains grafted to spherical particles. 34 The PABs, by contrast, contain monomer species that are oppositely charged in their ionized states. As a result, increasing ρ enhances electrostatic screening in the brushes and reduces repulsive interactions between similarly charged species. This screening effect causes ionization to become more favorable, leading to a noticeable increase in $\langle \alpha \rangle$ near the extremes of pH^{res} as ρ increases. ²⁷ Interestingly, similar shifts in ionization behavior have been observed in the polymer-dense coacervate phase formed when mixing two oppositely charged polymers in solution. 68-71

Variation in $\langle \alpha \rangle$ with pH^{res} leads to concomitant changes in the structure of the brushes. To characterize these changes, we calculated the average brush height, ^{24,72,73}

$$\langle h \rangle = \frac{\int_0^\infty z \rho_{\rm m}(z)}{\int_0^\infty \rho_{\rm m}(z)},\tag{21}$$

where $\rho_{\rm m}(z)$ is the density of monomers as a function of the distance from the grafting surface z (Fig. S5 in ESI). As expected, the height of the PEBs varies monotonically with pH^{res} for all grafting densities ρ (Fig. 3), exhibiting sigmoidal behavior similar to that observed for the degree of ionization $\langle \alpha \rangle$ (Fig. 2). At one extreme of pH^{res}, the degree of ionization $\langle \alpha \rangle \to 0$ for the PEBs, and $\langle h \rangle$ approaches that of a neutral brush with the same grafting density. At the other pH^{res} extreme, the PEBs fully ionize (i.e., $\langle \alpha \rangle \to 1$) and become maximally extended due to charge-charge repulsion along the chains.

For pH^{res} $\approx 4-10$, the PABs exhibit characteristic heights $\langle h \rangle$ less than those of the PEBs with the same grafting densities. The PABs are almost fully ionized in this pHres range (Fig. 2), and each polymer chain contains approximately an equal number of negatively and positively charged monomers. The oppositely charged monomers result in strong inter- and intra-chain charge-charge attractions that favor compact configurations. As observed in previous computational studies of strongly ionized PABs, this effect is more pronounced for sequences with larger block sizes, ⁷⁴ resulting in a decrease in height as block size increases. At the extremes of pHres, however, the PABs become increasingly negatively or positively charged as $\langle \alpha \rangle \rightarrow 0.5$ and only like monomers on the chains remain ionized. This loss of neutrality enhances the effects of charge-charge repulsion, resulting in increases in $\langle h \rangle$ beyond that of neutral brushes. Similar behavior has been previously reported in both experimental 75,76 and numerical 27,77 investigations of diblock PABs. The slight asymmetry in the response of $\langle h \rangle$ to changes in pH arises because the polymers are end grafted to the surface by their acidic block ²⁷ and because the disassociation constants for the acidic and basic monomers are not symmetric about $pH^{res} = 7$.

The brush height for the PAB with the alternating sequence $(KE)_{24}$ is similar to that of a neutral brush for $pH^{res} \approx 4-10$ and exhibits the least pronounced variations with pH^{res} . This behavior occurs because similarly charged monomers are maximally spaced in this sequence and thus charge-charge repulsion along the chains are strongly screened. Consequently, the change in $\langle h \rangle$ with pH^{res} increases with block size because larger fractions of similarly charged monomers are in close proximity. The effects of grafting density are less pronounced than those of monomer sequence. For a given PAB at a fixed pH^{res} , $\langle h \rangle$ increases with ρ due to stronger excluded volume effects. 24,25,78 The magnitude of the changes in $\langle h \rangle$ with pH^{res} for the PABs also decrease with increasing ρ because of enhanced electrostatic screening in denser systems and the correspondingly smaller changes in $\langle \alpha \rangle$ (Fig. 2).

Chain conformation was also characterized by computing the the shape factor $\langle R_e^2 \rangle/\langle R_g^2 \rangle$, where $\langle R_e^2 \rangle$ and $\langle R_g^2 \rangle$ are the mean squared chain end-to-end distance and radius of gyration, respectively (Fig. 4). 29,79 By definition, the shape factor is 6 for a Gaussian coil and 12 for a rodlike chain. The general trends in the shape factor closely follow those observed in the brush height (Fig. 3) and $\langle R_e^2 \rangle^{1/2}$ and $\langle R_g^2 \rangle^{1/2}$ (Figs. S6 and S7 in ESI). The shape factor reveals that the chain conformations in the PEBs are similar to those in a neutral system with the same grafting density when the degree of ionization is low and become more rodlike due to increased charge-charge repulsions as $\langle \alpha \rangle \rightarrow 1.0$ (Figs. 2 and 4).

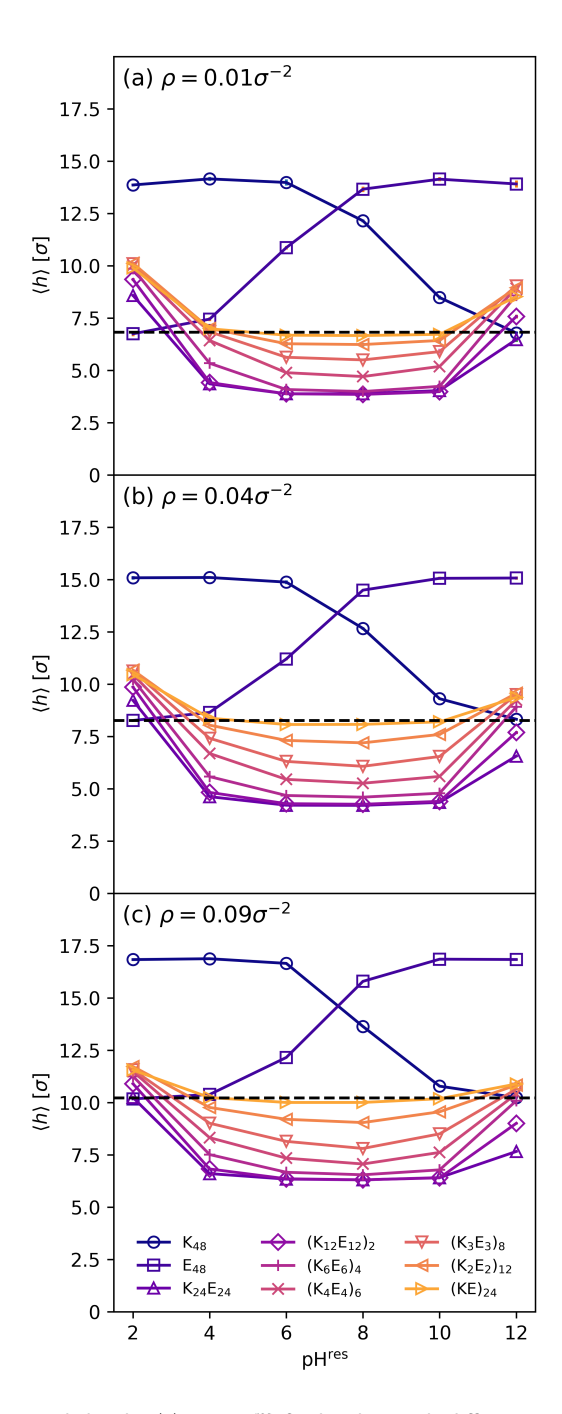


Fig. 3 Brush height $\langle h \rangle$ vs. pHres for brushes with different monomer sequences and grafting densities of $\rho=$ (a) 0.01, (b) 0.04, and (c) 0.09 $\sigma^{-2}.$ The dashed lines in each panel denote the height of a neutral brush with the same grafting density. Uncertainties are smaller than symbol size.

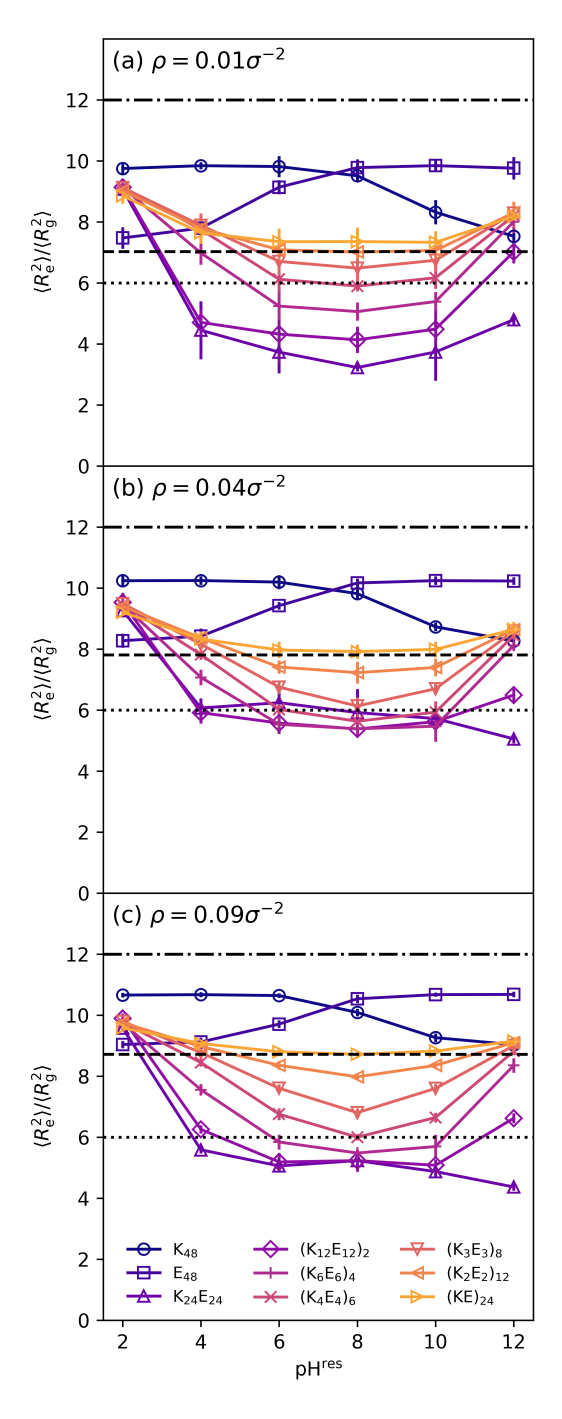


Fig. 4 Chain shape factor $\langle R_e^2 \rangle/\langle R_g^2 \rangle$ for brushes with different monomer sequences and grafting densities of $\rho=$ (a) 0.01, (b) 0.04, and (c) 0.09 σ^{-2} . $\langle R_e^2 \rangle$ and $\langle R_g^2 \rangle$ are the mean squared chain end-to-end distance and radius of gyration, respectively. Reference shape factor values are shown for a neutral brush with the same grafting density (dashed line), a Gaussian coil (dotted line), and a rigid rodlike chain (dash-dotted line). Where not visible, uncertainties are smaller than symbol size.

The shape factor for the PABs with the alternating sequence $(KE)_{24}$ exhibits a global minimum near $pH^{res}=8,$ where it assumes a value similar to that of the neutral brush with the same grafting density. For $pH^{res}\approx 4-10,$ the shape factor decreases as block size is increased from 1 to 24 (i.e., $(KE)_{24}$ to $K_{24}E_{24}).$ For block sizes larger than 4, the minimum in the shape factor is below that for a Gaussian coil, indicating that the chains adopt highly compact conformations in this pH^{res} range, consistent with the marked decrease in brush height observed under these conditions (Fig. 3).

The radius of gyration in the x-y plane parallel to the grafting surface $\langle R_{\rm g,xy}^2 \rangle^{1/2}$ is strongly affected by grafting density, pH, and monomer sequence (Fig. 5). At the grafting density $\rho = 0.01\sigma^{-2}$, $\langle R_{g,xy}^2 \rangle^{1/2}$ is significantly smaller than the half-spacing between grafting sites for all brushes, indicating that inter-chain interactions are relatively weak under these conditions. Indeed, the normalized in-plane monomer density distributions $\rho_{\rm m}(x,y)/\rho$ for adjacent grafting sites do not significantly overlap under these conditions, confirming that the polymer chains are highly localized and well-separated from each other (Fig. 6). The in-plane radius of gyration for the alternating sequence (KE)24 exhibits a global maximum near neutral pHres. The negative concavity increases as block size increases from 1 to 4 ((KE) $_{24}$ to (K $_4$ E $_4$) $_6$). Upon increasing block size further, the concavity becomes positive and a minimum develops in $\langle R_{g,xy}^2 \rangle^{1/2}$ near neutral pH^{res}. This behavior arises from a competition between the tendency of the chains to expand in the lateral direction as the brush height decreases and attractive intra-chain interactions that suppress fluctuations. The latter effect eventually becomes dominant as block size increases due to the strong electrostatic attractions between large, oppositely charged blocks, which cause the chains to partially fold back on themselves.

This interpretation is supported by analysis of the average intermonomer distance $\langle R_{ij} \rangle$ as a function of sequence separation in the chain |j-i| (Fig. 7; Fig. S8 in ESI). Near neutral pH^{res} = 8, where the PABs are fully charged, $\langle R_{ij} \rangle$ exhibits nonmonotonic behavior for systems with block sizes of 6 and larger (Fig. 7(a)). This behavior indicates partial backfolding of the chains and arises from attractive electrostatic interactions between blocks, consistent with that observed in computational and theoretical studies of the polyampholytes in solution with similar sequences. 80-84 It is at odds with the monotonic increasing behavior observed for neutral brushes, in which only excluded volume interactions between nonbonded monomers are present (Fig. 7(a)). Strong electrostatic repulsions between monomers along the chain backbones in the PEBs, by contrast, lead to a significantly faster monotonic increase in $\langle R_{ij} \rangle$ than observed for neutral brushes with the same grafting density.

Lastly, at grafting density $\rho=0.04\sigma^{-2}$, the typical $\langle R_{\rm g,xy}^2\rangle^{1/2}$ values are larger than the half-spacing between grafting sites, suggesting that both inter- and intra-chain interactions influence brush behavior under these conditions. In sharp contrast with the global minima observed near pH^{res} at lower grafting density, the $\langle R_{\rm g,xy}^2\rangle^{1/2}$ curves for the PABs with block sizes of 6, 12, and 24 ((K_6E_6)₄, ($K_{12}E_{12}$)₂, and $K_{24}E_{24}$, respectively) exhibit global maxima. We posit that the maxima developed in these systems

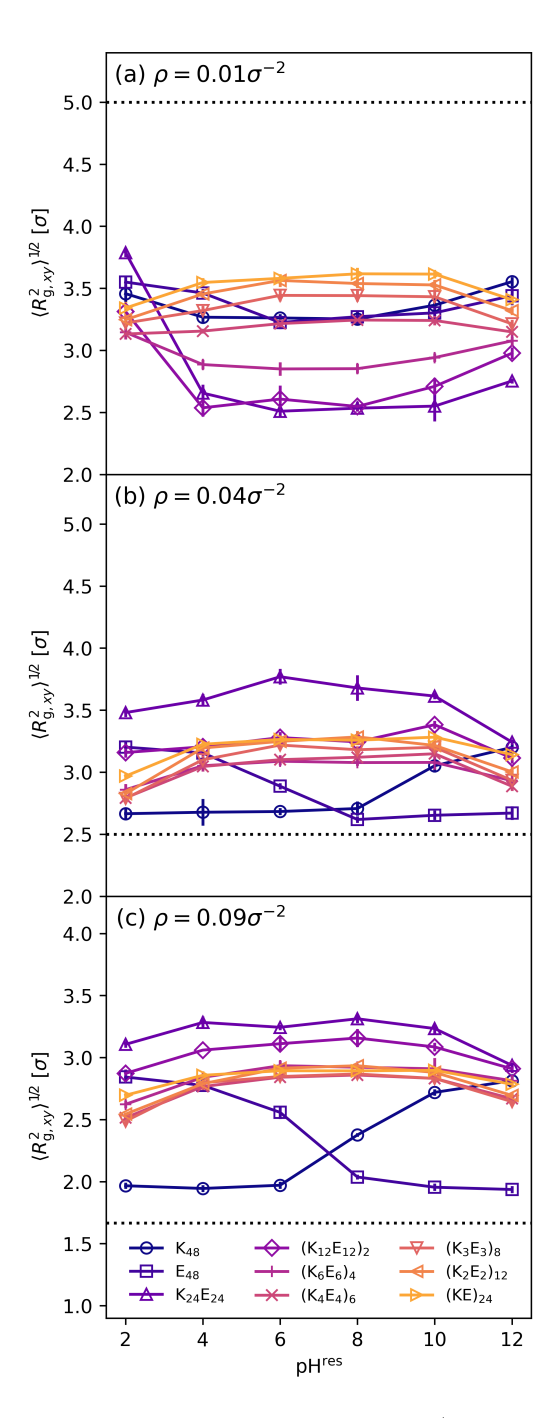


Fig. 5 Radius of gyration in the x-y plane $\langle R_{g,xy}^2 \rangle^{1/2}$ for brushes with different monomer sequences and grafting densities of $\rho=$ (a) 0.01, (b) 0.04, and (c) 0.09 σ^{-2} . The dotted line in each panel denotes the half-spacing between adjacent grafting sites. Where not visible, uncertainties are smaller than symbol size.

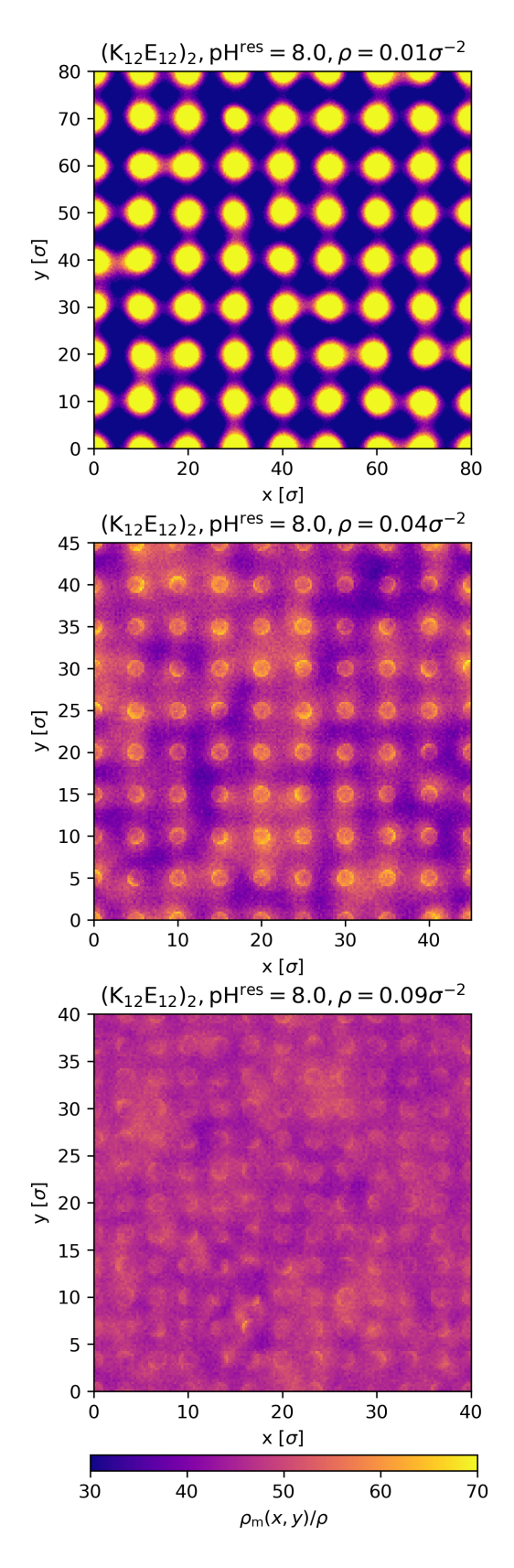


Fig. 6 Normalized monomer density $\rho_m(x,y)/\rho$ in the x-y plane at $pH^{res}=8$ for PABs with monomer sequence $(K_{12}E_{12})_2$ and grafting densities of $\rho=$ (a) 0.01, (b) 0.04, and (c) 0.09 σ^{-2} .

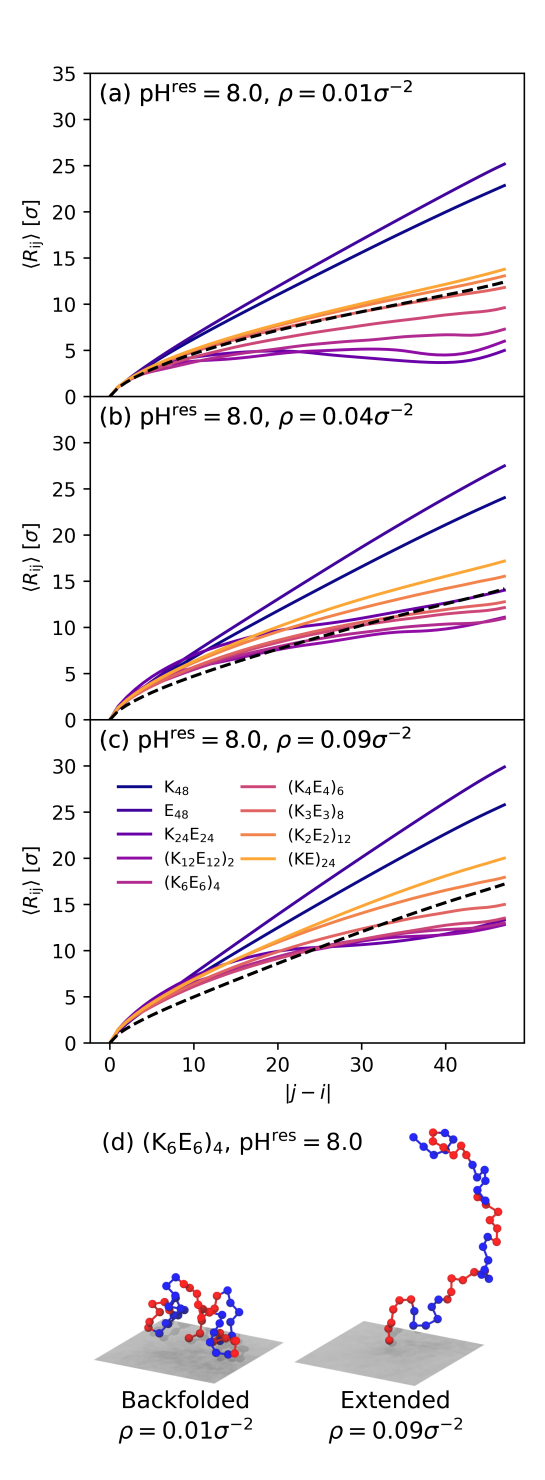


Fig. 7 Intermonomer distance $\langle R_{ij}\rangle$ as a function of sequence separation in the chain |j-i| at pHres =8 for brushes with different monomer sequences and grafting densities of $\rho=$ (a) 0.01, (b) 0.04, and (c) 0.09 σ^{-2} . The dashed lines in each panel denote $\langle R_{ij}\rangle$ for a neutral brush with the same grafting density. (d) Simulation snapshots of single $(K_6E_6)_4$ polymer chains from brushes with grafting densities of 0.01 and 0.09 σ^{-2} , illustrating the backfolded and extended conformations at these conditions, respectively.

from the presence of inter-chain electrostatic attractions between oppositely charged blocks on neighboring chains, which partially balance the strong intra-chain interactions and thus lead to enhanced lateral fluctuations near pHres where the brushes are fully ionized. This idea is consistent with the disappearance of the nonmonotonic behavior in $\langle R_{ij} \rangle$ for these systems, indicating that the intra-chain interactions are insufficiently dominant to result in partial backfolding of the chains (Fig. 7(b)). Additionally, the in-plane monomer density distributions reveal that the polymers become delocalized from their grafting sites as ρ increases from 0.01 to 0.04 σ^{-2} , corroborating the presence of enhanced lateral fluctuations (Fig. 6). Although the qualitative trends are similar at $\rho = 0.09\sigma^{-2}$, the values of $\langle R_{g,xy}^2 \rangle^{1/2}$ are slightly lower due to excluded volume interactions between neighboring chains at high grafting density that suppress lateral fluctuations.

Conclusions

We performed simulations using the grand reaction method to investigate the pH response of sequence-controlled PABs with alternating blocks of weakly acidic and basic monomers. The pH response of the PABs was found to depend sensitively on the sequence and deviate qualitatively from the behavior observed for PEBs consisting of poly-acids or bases. Specifically, variations in the degree of ionization, brush height, and chain shape factor with pH were found to increase with block size, with diblock sequences exhibiting the most pronounced pH response. Analysis of the intermonomer distances indicated that this behavior arises from attractive intra-chain interactions between oppositely charged blocks that result in partial backfolding of the chains, consistent with what has been reported for polyampholytes with similar sequences in solution. 80-84 Increasing grafting density, by contrast, was found to have a relatively modest effect on variations in brush ionization state and height with pH, but significantly affected the lateral structure of the PABs due to a partial balancing of the intra-chain interactions by electrostatic attractions between adjacent chains.

Although our study suggests that sequence-controlled PABs may be used to design smart surfaces with tunable pH responses, future investigations are needed to understand the effects of other key physical variables on their behavior. For example, recent studies have shown that salt ion concentration and valency and solvent quality can dramatically influence the behavior of charged brushes. 27,85,86 However, it remains unclear how these variables influence the sequence-dependent pH response of PABs. Additionally, here we focused on linear polyampholytes with alternating block sequences that are charge neutral when fully ionized. These sequences and architecture represents a very small fraction of the accessible design space, 87,88 which is challenging to extensively explore with the computationally intensive molecular simulation methods. Nonetheless, as has been successfully done for other polymer systems, 89,90 we posit that data from molecular simulation may be used to train machine learning models that can rapidly predict sequence-property relationships for PABs and thus aid in broader exploration of this design space. Finally, polymer sequence is likely to affect the dynamics of brushes across the stimulus-responsive range of pH but remains underexplored. Studies characterizing brush dynamics, their coupling to the motion of small molecules or particles, and the effects of hydrodynamic interactions, as have been performed for bulk polymer solutions, 91-93 are likely to provide insight into the design parameters required to control responsive transport of penetrants within brushes. By connecting solution conditions and brush structure to brush response, we anticipate that such studies will enable the design of tunable, stimulus-responsive soft interfaces.

Conflicts of interest

There are no conflicts to declare

Acknowledgements

We gratefully acknowledge Dr. Debra Audus (National Institute of Standards and Technology) for comments on the manuscript and the authors of Ref. 35 (Drs. Jonas Landsgesell, Pascal Hebbeker, Oleg Rud, Raju Lunkad, Peter Košovan, and Christian Holm) for providing example code for implementing the grand-reaction method. We thank the National Science Foundation (CBET-2113769, CBET-2113767, CBET-1751173 to JCC, ABM, and JCP, respectively) and the Welch Foundation (E-1869, C-2003-20190330, E-1882 to JCC, ABM, and JCP, respectively) for partial support of this work. Computational resources were generously provided by the Hewlett Packard Enterprise Data Science Institute at the University of Houston and the Texas Advanced Computing Center at the University of Texas at Austin.

Notes and references

- 1 E. N. Durmaz, S. Sahin, E. Virga, S. de Beer, L. C. P. M. de Smet and W. M. de Vos, ACS Applied Polymer Materials, 2021, 3, 4347-4374.
- 2 K. Qu, Z. Yuan, Y. Wang, Z. Song, X. Gong, Y. Zhao, Q. Mu, Q. Zhan, W. Xu and L. Wang, ChemPhysMater, 2022, 1, 294-309.
- 3 W.-L. Chen, R. Cordero, H. Tran and C. K. Ober, Macromolecules, 2017, 50, 4089-4113.
- 4 M. A. C. Stuart, W. T. S. Huck, J. Genzer, M. Müller, C. Ober, M. Stamm, G. B. Sukhorukov, I. Szleifer, V. V. Tsukruk, M. Urban, F. Winnik, S. Zauscher, I. Luzinov and S. Minko, Nature Materials, 2010, 9, 101–113.
- 5 J. C. Conrad and M. L. Robertson, Current Opinion in Solid State and Materials Science, 2019, 23, 1-12.
- 6 W. Choi, S. Park, J.-S. Kwon, E.-Y. Jang, J.-Y. Kim, J. Heo, Y. Hwang, B.-S. Kim, J.-H. Moon, S. Jung, S.-H. Choi, H. Lee, H.-W. Ahn and J. Hong, ACS Nano, 2021, 15, 6811-6828.
- 7 Y. Higaki, M. Kobayashi and A. Takahara, Langmuir, 2020, 36, 9015-9024.
- 8 Q. He, Y. Qiao, C. Medina Jimenez, R. Hackler, A. B. Martinson, W. Chen and M. V. Tirrell, Macromolecules, 2023, 1945-1953.
- 9 Q. Li, C. Wen, J. Yang, X. Zhou, Y. Zhu, J. Zheng, G. Cheng, J. Bai, T. Xu, J. Ji et al., Chemical Reviews, 2022, 122, 17073-
- 10 M. T. Bernards, G. Cheng, Z. Zhang, S. Chen and S. Jiang, Macromolecules, 2008, 41, 4216-4219.

- 11 J. B. Schlenoff, Langmuir, 2014, 30, 9625-9636.
- 12 K. Qu, Z. Yuan, Y. Wang, Z. Song, X. Gong, Y. Zhao, Q. Mu, Q. Zhan, W. Xu and L. Wang, *ChemPhysMater*, 2022, 294– 309.
- 13 S. Chen, Z. Cao and S. Jiang, *Biomaterials*, 2009, **30**, 5892–5896.
- 14 A. J. Keefe, K. B. Caldwell, A. K. Nowinski, A. D. White, A. Thakkar and S. Jiang, *Biomaterials*, 2013, **34**, 1871–1877.
- 15 A. K. Nowinski, F. Sun, A. D. White, A. J. Keefe and S. Jiang, *Journal of the American Chemical Society*, 2012, **134**, 6000–6005.
- 16 M. Piatkovsky, H. Acar, A. B. Marciel, M. Tirrell and M. Herzberg, *Journal of Membrane Science*, 2018, 549, 507– 514.
- 17 H. Ye, J. Che, R. Huang, W. Qi, Z. He and R. Su, *Langmuir*, 2020, **36**, 1923–1929.
- 18 K. H. A. Lau, T. S. Sileika, S. H. Park, A. M. Sousa, P. Burch, I. Szleifer and P. B. Messersmith, *Advanced Materials Inter*faces, 2015, 2, 1400225.
- 19 C. Li, C. Liu, M. Li, X. Xu, S. Li, W. Qi, R. Su and J. Yu, *Biomacromolecules*, 2020, **21**, 2087–2095.
- 20 T. Ederth, M. Lerm, B. Orihuela and D. Rittschof, *Langmuir*, 2018, **35**, 1818–1827.
- 21 J. Dinic, A. B. Marciel and M. V. Tirrell, *Current Opinion in Colloid & Interface Science*, 2021, **54**, 101457.
- 22 M. Li, B. Zhuang and J. Yu, *Macromolecules*, 2021, **54**, 9565–9576.
- 23 D. L. Cheung and K. H. A. Lau, *Langmuir*, 2018, **35**, 1483–1494.
- 24 M. Baratlo and H. Fazli, *The European Physical Journal E*, 2009, **29**, 131–138.
- 25 Q. Cao and H. You, Langmuir, 2015, 31, 6375-6384.
- 26 Q. Cao and H. You, Polymer, 2017, 113, 233-246.
- 27 D. Prusty, R. Nap, I. Szleifer and M. O. De La Cruz, *Soft Matter*, 2020, **16**, 8832–8847.
- 28 F. Weik, R. Weeber, K. Szuttor, K. Breitsprecher, J. de Graaf, M. Kuron, J. Landsgesell, H. Menke, D. Sean and C. Holm, *The European Physical Journal Special Topics*, 2019, 227, 1789–1816.
- 29 M. J. Stevens and K. Kremer, *The Journal of Chemical Physics*, 1995, **103**, 1669–1690.
- 30 H. J. Limbach and C. Holm, *The Journal of Chemical Physics*, 2001, **114**, 9674–9682.
- 31 Q. Liao, J.-M. Y. Carrillo, A. V. Dobrynin and M. Rubinstein, *Macromolecules*, 2007, **40**, 7671–7679.
- 32 A. V. Dobrynin, *Current Opinion in Colloid & Interface Science*, 2008, **6**, 376–388.
- 33 J.-M. Y. Carrillo and A. V. Dobrynin, *Macromolecules*, 2011, 44, 5798–5816.
- 34 S. Barr and A. Panagiotopoulos, *The Journal of Chemical Physics*, 2012, **137**, 144704.
- 35 J. Landsgesell, P. Hebbeker, O. Rud, R. Lunkad, P. Kosovan and C. Holm, *Macromolecules*, 2020, **53**, 3007–3020.

- 36 R. Stano, P. Kosovan, A. Tagliabue and C. Holm, *Macro-molecules*, 2021, 54, 4769–4781.
- 37 O. V. Rud, J. Landsgesell, C. Holm and P. Kosovan, *Desalination*, 2021, **506**, 114995.
- 38 J. J. Madinya, L.-W. Chang, S. L. Perry and C. E. Sing, *Molecular Systems Design & Engineering*, 2020, **5**, 632–644.
- 39 A. M. Rumyantsev, A. Johner and J. J. de Pablo, *ACS Macro Letters*, 2021, **10**, 1048–1054.
- 40 W. H. Shi, R. S. Adhikari, D. N. Asthagiri and A. B. Marciel, *ACS Macro Letters*, 2023, **12**, 195–200.
- 41 D. Iqbal, J. Yan, K. Matyjaszewski and R. D. Tilton, *Colloid and Polymer Science*, 2020, **298**, 35–49.
- 42 S. Christau, T. Moller, Z. Yenice, J. Genzer and R. von Klitzing, *Langmuir*, 2014, **30**, 13033–13041.
- 43 B. Lego, W. Skene and S. Giasson, *Macromolecules*, 2010, 43, 4384–4393.
- 44 J. D. Weeks, D. Chandler and H. C. Andersen, *The Journal of Chemical Physics*, 1971, **54**, 5237–5247.
- 45 K. Kremer and G. S. Grest, *The Journal of Chemical Physics*, 1990, **92**, 5057–5086.
- 46 R. B. Bird, R. C. Armstrong and O. Hassager, *Dynamics of polymeric liquids*. Vol. 1 and 2, Wiley, 1987.
- 47 R. W. Hockney and J. W. Eastwood, *Computer Simulation using Particles*, 1988, 267–304.
- 48 A. Arnold, J. de Joannis and C. Holm, *The Journal of Chemical Physics*, 2002, **117**, 2496–2502.
- 49 J. de Joannis, A. Arnold and C. Holm, *The Journal of Chemical Physics*, 2002, **117**, 2503–2512.
- 50 W. Smith and B. Triska, *The Journal of Chemical Physics*, 1994, 100, 3019–3027.
- 51 J. K. Johnson, A. Z. Panagiotopoulos and K. E. Gubbins, *Molecular Physics*, 1994, **81**, 717–733.
- 52 D. Frenkel and B. Smit, *Understanding molecular simulation:* from algorithms to applications, Elsevier, 2001, vol. 1.
- 53 D. Adams, Molecular Physics, 1974, 28, 1241-1252.
- 54 C. E. Reed and W. F. Reed, *The Journal of Chemical Physics*, 1992, **96**, 1609–1620.
- 55 T. Curk, J. Yuan and E. Luijten, *The Journal of Chemical Physics*, 2021, 044122.
- 56 J. Landsgesell, L. Nová, O. Rud, F. Uhlík, D. Sean, P. Hebbeker, C. Holm and P. Košovan, *Soft Matter*, 2019, **15**, 1155–1185.
- 57 V. Z. Spassov, H. Luecke, K. Gerwert and D. Bashford, *Journal of Molecular Biology*, 2001, **312**, 203–219.
- 58 K. P. Kilambi and J. J. Gray, *Biophysical Journal*, 2012, **103**, 587–595.
- 59 B. Widom, *The Journal of Chemical Physics*, 1963, **39**, 2808–2812.
- 60 J. Jackson and L. Klein, *The Physics of Fluids*, 1964, 7, 228–231.
- 61 N. Metropolis, A. W. Rosenbluth, M. N. Rosenbluth, A. H. Teller and E. Teller, *The Journal of Chemical Physics*, 1953, **21**, 1087–1092.
- 62 D. A. Kofke and E. D. Glandt, Molecular Physics, 1988, 64, 1105–1131.

- 63 V. S. Rathee, H. Sidky, B. J. Sikora and J. K. Whitmer, Journal of the American Chemical Society, 2018, 140, 15319–15328.
- 64 V. S. Rathee, B. J. Sikora, H. Sidky and J. K. Whitmer, Materials Research Express, 2018, 5, 014010.
- 65 V. S. Rathee, H. Sidky, B. J. Sikora and J. K. Whitmer, Polymers, 2019, 11, 183.
- 66 P. Gong, T. Wu, J. Genzer and I. Szleifer, Macromolecules, 2007, 40, 8765–8773.
- 67 K. N. Witte, S. Kim and Y.-Y. Won, The Journal of Physical Chemistry B, 2009, 113, 11076–11084.
- 68 A. Salehi and R. G. Larson, Macromolecules, 2016, 49, 9706-9719.
- 69 V. S. Rathee, A. J. Zervoudakis, H. Sidky, B. J. Sikora and J. K. Whitmer, The Journal of Chemical Physics, 2018, 148, 114901.
- 70 A. R. Knoerdel, W. C. Blocher McTigue and C. E. Sing, The Journal of Physical Chemistry B, 2021, 125, 8965-8980.
- 71 Z. A. Digby, M. Yang, S. Lteif and J. B. Schlenoff, Macromolecules, 2022, 55, 978-988.
- 72 W. M. de Vos and F. A. Leermakers, Polymer, 2009, 50, 305-
- 73 M. Murat and G. S. Grest, Macromolecules, 1989, 22, 4054-4059.
- 74 Baratlo, M. and Fazli, H., Eur. Phys. J. E, 2009, 29, 131–138.
- 75 N. Ayres, C. D. Cyrus and W. J. Brittain, Langmuir, 2007, 23, 3744-3749.
- 76 N. Srinivasan, M. Bhagawati, B. Ananthanarayanan and S. Kumar, Nature Communications, 2014, 5, 5145.
- 77 L.-J. Qu, X. Man, C. C. Han, D. Qiu and D. Yan, The Journal of Physical Chemistry B, 2012, 116, 743–750.
- 78 S. Misra, S. Varanasi and P. Varanasi, Macromolecules, 1989, 22, 4173-4179.
- 79 M. Rubinstein and R. H. Colby, Polymer Physics, Oxford Uni-

- versity Press, Oxford, 2007.
- 80 R. K. Das and R. V. Pappu, Proceedings of the National Academy of Sciences, 2013, 110, 13392-13397.
- 81 L. Sawle and K. Ghosh, The Journal of Chemical Physics, 2015, **143**, 08B615.
- 82 D. S. Devarajan, S. Rekhi, A. Nikoubashman, Y. C. Kim, M. P. Howard and J. Mittal, Macromolecules, 2022, 55, 8987-8997.
- 83 S. P. O. Danielsen, J. McCarty, J.-E. Shea, K. T. Delaney and G. H. Fredrickson, Proceedings of the National Academy of Sciences, 2019, 116, 8224-8232.
- 84 A. M. Rumyantsev, N. E. Jackson, A. Johner and J. J. de Pablo, Macromolecules, 2021, 54, 3232-3246.
- 85 N. E. Jackson, B. K. Brettmann, V. Vishwanath, M. Tirrell and J. J. de Pablo, ACS Macro Letters, 2017, 6, 155–160.
- 86 J. Yu, N. E. Jackson, X. Xu, B. K. Brettmann, M. Ruths, J. J. de Pablo and M. Tirrell, Science Advances, 2023, 3, eaao1497.
- 87 J. P. Berezney, A. B. Marciel, C. M. Schroeder and O. A. Saleh, Physical Review Letters, 2017, 119, 127801.
- 88 G. Gunkel, M. Weinhart, T. Becherer, R. Haag and W. T. S. Huck, Biomacromolecules, 2011, 12, 4169-4172.
- 89 M. A. Webb, N. E. Jackson, P. S. Gil and J. J. de Pablo, Science Advances, 2023, 6, eabc6216.
- 90 A. Statt, D. C. Kleeblatt and W. F. Reinhart, Soft Matter, 2021, **17**, 7697–7707.
- 91 R. Chen, R. Poling-Skutvik, A. Nikoubashman, M. P. Howard, J. C. Conrad and J. C. Palmer, Macromolecules, 2018, 51, 1865-1872.
- 92 R. Chen, R. Poling-Skutvik, M. P. Howard, A. Nikoubashman, S. A. Egorov, J. C. Conrad and J. C. Palmer, Soft Matter, 2019, **15**, 1260–1268.
- 93 M. P. Howard, A. Nikoubashman and J. C. Palmer, Current Opinion in Chemical Engineering, 2019, 23, 34–43.